ADVANCED MATERIALS
www.advmat.de

Dirac-Like Fermions Anomalous Magneto-Transport in a Spin-Polarized Oxide 2D Electron System

Yu Chen, Maria D'Antuono, Mattia Trama, Daniele Preziosi, Benoit Jouault, Frédéric Teppe, Christophe Consejo, Carmine A. Perroni, Roberta Citro, Daniela Stornaiuolo,* and Marco Salluzzo**

In a 2D electron system (2DES) the breaking of the inversion, time-reversal and bulk crystal-field symmetries is interlaced with the effects of spin-orbit coupling (SOC) triggering exotic quantum phenomena. Here, epitaxial engineering is used to design and realize a 2DES characterized simultaneously by ferromagnetic order, large Rashba SOC and hexagonal band warping at the (111) interfaces between $LaAlO_3$, $EuTiO_3$, and $SrTiO_3$ insulators. The 2DES displays anomalous quantum corrections to the magneto-conductance driven by the time-reversal-symmetry breaking occurring below the magnetic transition temperature. The results are explained by the emergence of a non-trivial Berry phase and competing weak anti-localization/weak localization back-scattering of Dirac-like fermions, mimicking the phenomenology of gapped topological insulators. These findings open perspectives for the engineering of novel spin-polarized functional 2DES holding promises in spin-orbitronics and topological electronics.

1. Introduction

Low dimensional electron systems can display exotic physical phenomena governed by the emergence of a non-trivial Berry curvature. The latter is linked to a band structure locally mimicking the dispersion relations of relativistic particles. The effects of these Dirac-like fermions in a 2DES are revealed when the chemical potential is tuned near the avoided crossing of Rashba-like SOC split bands. In 3D-topological insulators (TIs) Dirac fermions drive intriguing quantum transport properties, such as the quantum anomalous Hall effect,[1,2] topological phase transitions[3] and changeovers from weak anti-localization (WAL) to weak localization (WL) quantum corrections to the magneto-conductance (MC).[4–6] In particular, the hexagonal band warping of most 3D-TIs can trigger a net out-of-plane spin polarization induced by in-plane magnetic fields, and the opening of scattering channels between multiple pairs of stationary points with opposite momenta.[7] When a time-reversal-symmetry (TRS) breaking is introduced in such systems,[4–6] the opening of a magnetic gap leads to an extra WL scattering channel, beside the WAL spin-orbit scattering associated to a π Berry phase[8,9] (see **Figure 1**a–c).

Among low dimensional electron systems, 2DESs at the oxide interfaces are particularly appealing, as they can be opportunely engineered by epitaxy to host novel quantum

Y. Chen, D. Stornaiuolo, M. Salluzzo
CNR-SPIN
Complesso Univ. Monte S. Angelo
Naples I-80126, Italy
E-mail: yu.chen@spin.cnr.it; daniela.stornaiuolo@unina.it; marco.salluzzo@spin.cnr.it

The ORCID identification number(s) for the author(s) of this article can be found under https://doi.org/10.1002/adma.202410354

[+]Present address: Instituto de Microelectronica de Barcelona (IMB-CNM, CSIC), Campus UAB, 08193 Bellaterra, Spain

[++]Present address: Institute for Theoretical Solid State Physics, IFW Dresden, Helmholtzstr, 20, 01069 Dresden, Germany

DOI: 10.1002/adma.202410354

M. D'Antuono[+], C. A. Perroni, D. Stornaiuolo
Department of Physics
University of Naples Federico II
Complesso Univ. Monte S. Angelo
Naples I-80126, Italy

M. Trama[++], R. Citro
Department of Physics
Universitá degli studi di Salerno
Via Giovanni Paolo II, 132, Salerno I-84084, Italy

D. Preziosi
Institut de Physique et Chimie des Matériaux de Strasbourg
UMR 7504 CNRS, Strasbourg F-67034, France

B. Jouault, F. Teppe, C. Consejo
Laboratoire Charles Coulomb
UMR 5221, CNRS, Université de Montpellier
Montpellier F-34095, France

R. Citro
CNR-SPIN
Via Giovanni Paolo II, 132, Salerno I-84084, Italy

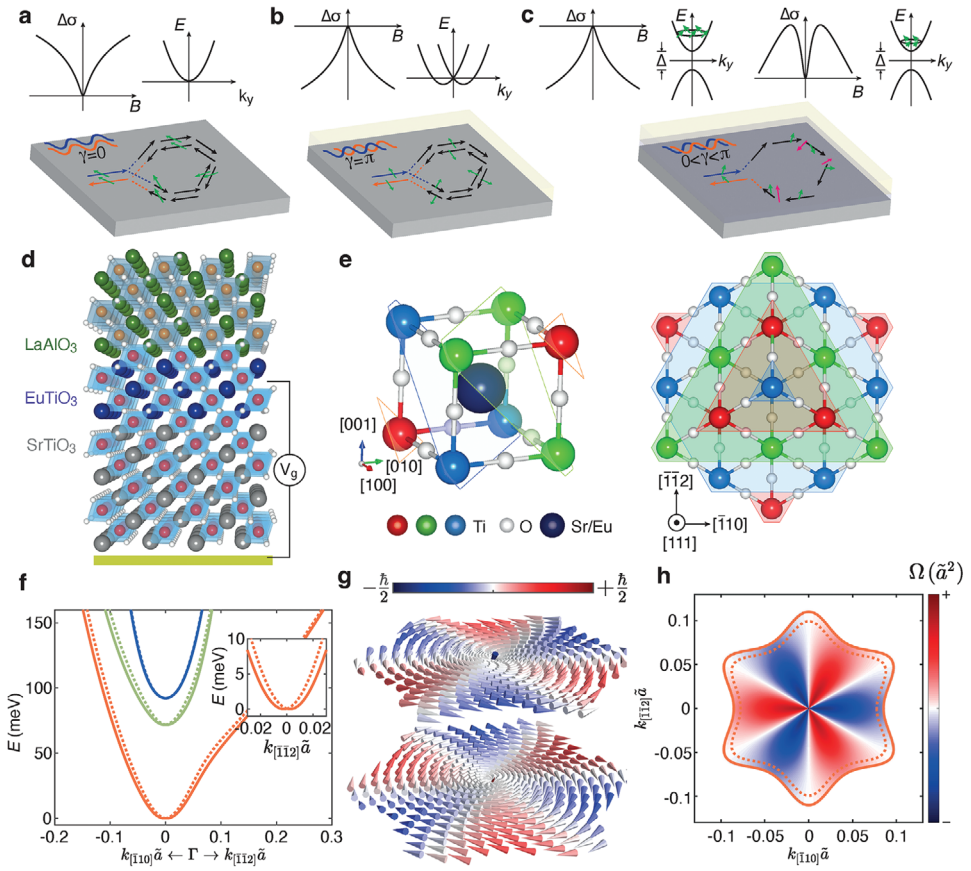

Figure 1. a) Sketches of WL in a system without spin-momentum locking, e.g., disordered metals with constructive interference of self-crossing loops and a zero Berry phase. b) WAL in SOC systems, e.g., topological insulators and oxide interfaces, due to a destructive interference and a π Berry phase. c) Competing WL and WAL with a non-trivial Berry phase at low doping (right) in gapped Dirac systems, e.g., magnetically doped TIs.[4] d) Sketch of the LAO/ETO/STO heterostructure with a back-gate electrode. e) The (Eu, Sr)TiO_3 lattice (left) and its projection (right) on the (111) interface/surface plane. Along the [111] interface/surface normal, the system consists of three non-equivalent layers of Ti atoms (red, green, blue), with the two perpendicular $[\bar{1}\bar{1}2]$ and $[\bar{1}10]$ crystallographic axes. f) Electronic band structure, E(k) of (111) interfaces, showing bands with a_{1g} (red) and $e^{\pi}_{g\pm}$ (green, blue) orbital character, together with their Rashba-like split counterparts (dark dotted lines). Throughout this letter, $k\tilde{a}$ are in units of π, where $\tilde{a} = \sqrt{2/3}a_0$ with the cubic STO lattice constant $a_0 = 3.905$Å. g) Spin arrangements of the lowest spin-split bands composed of a_{1g} orbitals, exhibiting the emergence of an out-of-plane component induced by the hexagonal warping effect. The magnitude of the out-of-plane component is shown using a blue (spin down) to red (spin-up) color gradient-scale. h) Corresponding Fermi contours shown as continuous/dotted lines and Berry curvature color map of a sub-band at $E_F = 60$ meV.

phenomena, from unconventional superconductivity[10–12] to exotic magnetism and multiferroic behavior.[13] In the 2DES at the (001) interfaces between $LaAlO_3$ (LAO), $EuTiO_3$ (ETO), and $SrTiO_3$ (STO) (LAO/ETO/STO), for instance, ferromagnetic correlations, due to the magnetic ordering of Eu^{2+} ($4f^7$) ions, coexist with a relatively large Rashba-like SOC and unconventional superconductivity.[11,14]

Recently, the study of (111) STO-based interfaces unveiled a large and unexpected in-plane second order bi-linear magnetoresistance and anomalous Hall effect, induced by a large in-plane magnetic field.[15–17] The results, in part linked to the hexagonal band-warping of (111) heterostructures,[16] were interpreted as signatures of an out-of-plane spin-polarization and non-trivial Berry curvature nearby the Dirac-like point formed at crossing bands split, at finite momentum, by the Rashba-SOC.

Here, we show how epitaxial engineering of oxide heterostructures enables the realization of a rare example of oxide 2DES characterized by hexagonal band-warping and breaking of the inversion and time-reversal symmetries, which give rise to a non-trivial Berry phase ($\gamma \notin \{0, \pi\}$) without the application of in-plane magnetic fields. This non-trivial Berry phase is manifested directly in the quantum corrections to the first-order MC which shows competing WL/WAL scattering channels of Dirac-like fermions, with a phenomenology analogous to that of magnetically doped 3D-TIs.[4–6]

2. Results and Discussion

The 2DES was realized by sequential epitaxial deposition of 3 unit cells (uc) delta-doping (111) ETO layer and 14 uc LAO on a Ti-terminated (111) STO single crystal (see Experimental Section; Figure S1a, Supporting Information). Magneto-transport properties were studied on Hall-bar devices patterned using photolithography and ion beam etching at low temperature[18] (see

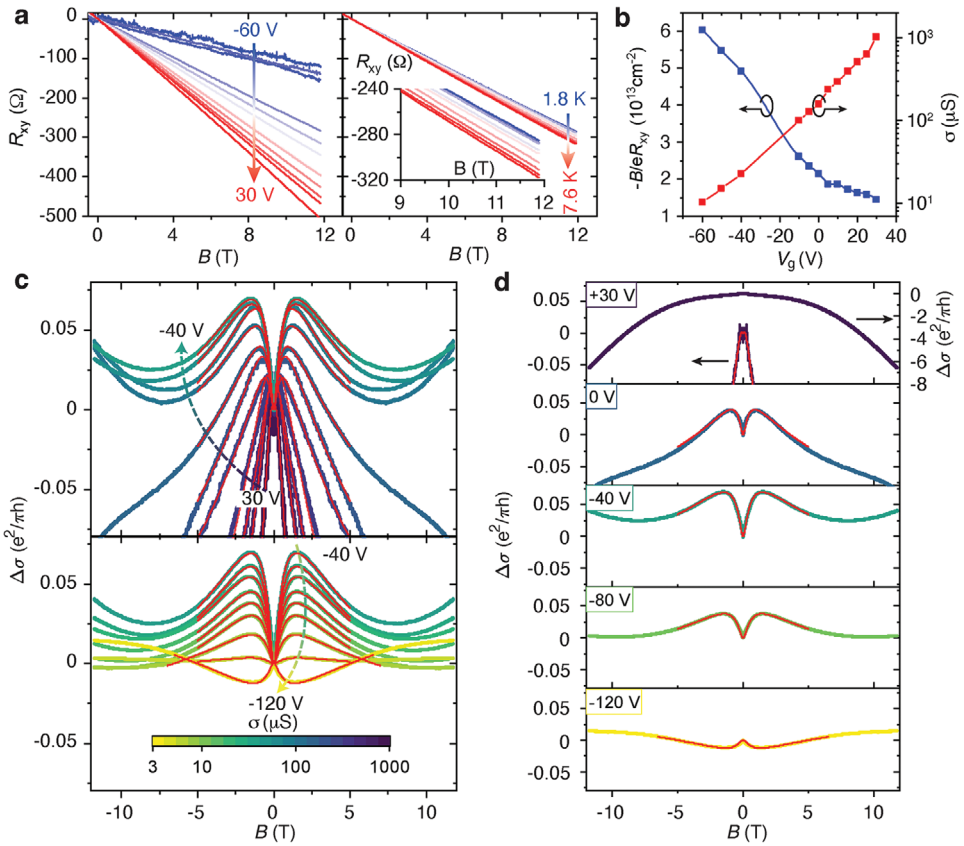

Figure 2. a) Gate voltage (at 1.8 K) and temperature (at $V_g = -10$ V) dependence of the Hall effect on a Hall-bar oriented along the [$\bar{1}$10] crystallographic direction. The inset is a zoomed-in view. b) Gate voltage dependence of the inverse Hall coefficient and sheet conductance. c) MC as function of gate voltages in the range +30 V to –40 V (upper panel) and –40 V to –120 V (lower panel). MC data in full voltage range is also shown in Figure S5 (Supporting Information). The color-code of each MC data corresponds to the sheet conductance shown in the colorbar ($\sigma \approx 1\,mS - 2.9\,\mu S$). Red lines are the best fits using Equation (1). d) Extracted MC data from the data set and their fits, at 30, 0, –40, –80, and –120 V, to highlight the evolution of the peak-shoulder feature as function of the gate voltage. The MC at +30 V in the full range is displayed in the right axis.

Experimental Section). Transport characterizations[19] confirm the formation of a 2DES with a sheet resistance temperature dependence similar to that of (001) and (111) LAO/STO heterostructures (Figure S1b, Supporting Information). Tuning of the chemical potential was achieved by back-gating, as schematically shown in Figure 1d.

(111) STO-based oxide 2DES can be described as repetition of three inequivalent Ti-layers stacked along the [111] vector, i.e., perpendicular to the interface, arranged in a hexagonal lattice[20–23] (Figure 1e). Inversion symmetry breaking gives rise to a D_{3d} trigonal symmetry, resulting in hybridized t_{2g} Ti-orbitals forming a_{1g}, e_g^{π} states[24] (Figure 1f; Figure S2a,b, Supporting Information). The trigonal crystal field has several consequences on the electronic band structure of the 2DES. First, as shown by tight-binding calculations (Note SI, Supporting Information), the Fermi surface of the lowest-energy bands exhibits a snowflake shape and a hexagonal band warping in a wide range of chemical potentials, affecting the electronic and transport properties.[22] Second, the hexagonal warping brings about an out-of-plane spin textures (see Figure 1g and refs. [15, 16, 23]) and a Berry curvature with alternating positive and negative values around the Brillouin zone, as illustrated by numerical calculations for the lowest band with a_{1g} orbital character (Figure 1h). This Berry curvature leads to an overall π Berry phase (Note SII, Supporting Information). As a result, pure WAL corrections to the low field MC are expected in these (111) systems that do not have a TRS breaking.[12,16,17]

On the other hand, (111) LAO/ETO/STO is characterized by ferromagnetically ordered Eu-ions, as confirmed by X-ray magnetic circular dichroism and SQUID magnetization measurements, with a ferromagnetic Tc of about 7.5K (see Figure S3, Supporting Information, and ref. [19]). The interaction between Eu-4f spins and Ti-3d moments induces a spin-polarization in the 2DES. Moreover, the trigonal crystal field splitting in this system is three times larger than the one of the (111) LAO/STO system,[24] enhancing the band splitting between the lowest a_{1g} and e_g^{π} derived bands. The enhanced splitting and the TRS-breaking driven by the ferromagnetic order are expected to induce novel quantum states, distinct from non-magnetic 2DES.

To study the low temperature physics of (111) LAO/ETO/STO, we performed an extensive study of the gate-voltage dependent magneto-transport properties of the system (**Figure 2**). In Figure 2a we show the Hall effect data measured as function of the gate voltage and temperature.The Hall-effect resistivity is

overall linear, however a closer look to the data shows a deviation from the linear behavior in the low field region, as highlighted by the derivative of the Hall effect (see Figure S4 and Note SIII, Supporting Information). This deviation is due to the presence of an anomalous Hall effect contribution due to the magnetism of the 2DES.[11,14] The anomalous component, R_{AHE}, extracted by subtracting the Hall effect slope around 4 Tesla from the transverse resistance R_{xy}, decreases as function of the gate-voltage, but is present in the whole range of gates explored, up to $V_g = +30$V (see Figure S4, Supporting Information). Above 4 Tesla the Hall effect is linear up to $V_g = +10$V, suggesting mostly single-band transport of electrons belonging to the lowest a_{1g} band. For larger gate voltages an additional curvature is observed indicating the emergence of another band contributing to the transport properties. The inverse Hall coefficient decreases when increasing the gate voltage (Figure 2b) that is opposite to the behavior observed in (001) oxide interfaces, where it reflects the accumulation of electron-carriers with the increase of the chemical potential. However, in (111) oxide heterostructures, the inverse Hall coefficient does not correspond to the electron carrier density, as also shown in ref. [22]. This result is a direct consequence of the band-warping, i.e., the non-parabolic nature of the a_{1g} band. The snowflake Fermi contours of this band give rise to regions having positive and negative curvatures, thus opposite Fermi velocities, akin to (111) LAO/STO interfaces in the low doping regime (see ref. [22] and Note SIV, Supporting Information).

In Figure 2(c,d) we show the gate voltage V_g dependence of the anomalous MC of (111) LAO/ETO/STO. At large negative gate voltage, i.e., –120 V, the MC is negative at low fields, similarly to what happens in the presence of WAL corrections (Figure 2d bottom panel). Increasing the gate voltage, the shape changes drastically and the MC becomes positive with a cusp-like shape, followed by a peak and a shoulder. The peak to shoulder feature increases with V_g, reaches a maximum at $V_g = -40$ V, and then decreases again until it almost (but not completely) disappears at +30 V (Figure 2d upper panel; see also Figure S5, Supporting Information). A similar anomaly is also observed in parallel field (see Figure S6, Supporting Information), which excludes an explanation based on a combination of suppressed quantum localization and reduced magnetic scattering,[25] and other negative MC terms like the classical parabolic orbital term (see Note SV, Supporting Information). Moreover, the anomalous positive cusp-like shape is remarkably different from the positive WL or the negative cusp-like WAL corrections observed in non-magnetic 2DES at the (001) and (111) LAO/STO[12,16,26] and $LaTiO_3$/STO interfaces.[17] The latter were well explained by the models of Hikami–Larkin–Nagaoka, Iordanskii–Lyanda–Geller–Pikus, or Maekaewa–Fukuyama.[27–29] On the other hand, the MC data of (111)LAO/ETO/STO (Figure 2c,d) are reminiscent of the phenomenology observed in the magneto-transport of magnetically doped 3D-TIs,[5] where it was attributed to competing WAL and WL channels induced by the opening of a magnetic gap Δ (see Figure 1c), and well reproduced by the formula derived in ref. [4]:

$$\delta\sigma(B) = \sum_{i=0,1} \frac{\alpha_i e^2}{\pi h}\left[\Psi\left(\frac{\ell_B^2}{\ell_{\phi i}^2}+\frac{1}{2}\right) - \ln\left(\frac{\ell_B^2}{\ell_{\phi i}^2}\right)\right] \quad (1)$$

where Ψ is the Digamma function, $\ell_B^2 = \hbar/4eB$ and $\ell_{\phi i}$ are the effective phase coherence lengths. The pre-factors α_0 and α_1, with opposite signs, represent the weights of the WAL and WL channels contributions. As shown in Figure 2c, where the fitting-curves are displayed as red-lines, Equation (1) captures well the data in the full range of gate voltages. As for 3D-TIs,[4] both α_i and $\ell_{\phi i}$ are expected to be function of the magnetic gap Δ and chemical potential E_F (see Figure S7, Supporting Information). The good agreement between the data and Equation (1) shown in Figure 2c,d indicates that the low temperature anomalous MC is explained by two competing WL and WAL scattering channels related to the magnetic gap Δ opening, each contributing to the MC quantum corrections.

In this framework, a purely WAL MC is predicted upon closing of the magnetic gap, which should take place approaching the FM transition of the system. In order to verify the link between the anomalous MC and the magnetism of the 2DES, in **Figure 3**a,b we show the peak-shoulder feature evolution as a function of the temperature at different gate voltages. By increasing the temperature, the MC-shape changes completely within few Kelvins and a negative MC, i.e., WAL, is recovered at temperatures in the range between 5 and 8 K, compatible with the fading away of magnetic correlations induced by the Eu^{2+} magnetic order (Tc between 5 and 10 K).[11,30] Thus the experimental results show that the anomalous MC is linked to the magnetic gap, that is, the band topology character.

As mentioned above, in magnetically doped 3D-TIs this band topology gives rise to a non-trivial Berry phase (see Figure 1c and ref. [4]). Now we introduce a minimal model including Rashba-split bands derived from the lowest a_{1g} orbital, a hexagonal warping term, and a magnetic exchange interaction related to the magnetic correlations in the 2DES. It is worth noting that within this minimal model, the hexagonal warping approximates well the band-structure of the (111) 2DES only at low values of the momentum (Figure S2a, Supporting Information). However, it has the advantage to provide analytical expressions for most of the quantities, which helps in understanding the main consequences of the interplay between Rashba-SOC, TRS-breaking, and the breaking of the bulk (D_{4h}) crystal-field symmetry into the D_{3d} symmetry.

Magnetic correlations in the 2DES are included by adding an in-plane ferromagnetic magnetization of the form $H_{FM} = \mathbf{h}_{||}\cdot\vec{\sigma} = \epsilon_{||}(\sigma_x\cos\psi + \sigma_y\sin\psi)$ (Note SVI, Supporting Information). Here ψ is the angle between the magnetization direction and the in-plane axis $\hat{x}$ ($[\bar{1}10]$), and $\mathbf{h}_{||}$ is the effective parallel field associated to the in-plane magnetic exchange $\epsilon_{||}$. The energy band dispersion assumes the form $E_\pm = \hbar^2\mathbf{k}^2/2m^* \pm \sqrt{\alpha^2k^6\cos^2(3\phi)+\lambda^2\tilde{k}^2}$, where $\tan(\phi) = k_y/k_x$, $\tilde{k}^2 = (k_x + \epsilon_{||}\sin\psi/\lambda)^2 + (k_y - \epsilon_{||}\cos\psi/\lambda)^2$, m^* is the effective mass, λ is the Rashba-SOC strength, and α is the warping parameter (Note SII, Supporting Information). In the presence of the internal in-plane magnetic exchange, a magnetic gap $\Delta = 2\alpha(\epsilon_{||}/\lambda)^3\sin(3\psi)$ opens up because the warping term couples the in-plane magnetization to the out-of-plane spin (**Figure 4**a,c), except for $\psi = 2\pi n/6$, i.e., along $[\bar{1}10]$ (Note SVI and Figure S9, Supporting Information). The Dirac-like point is then shifted from the center of Brillouin zone to the $\mathbf{k}^* = \hat{z}\times\mathbf{h}_{||}/\lambda$ position, where $\hat{z}$ is the unit vector along the [111] direction, leading to a

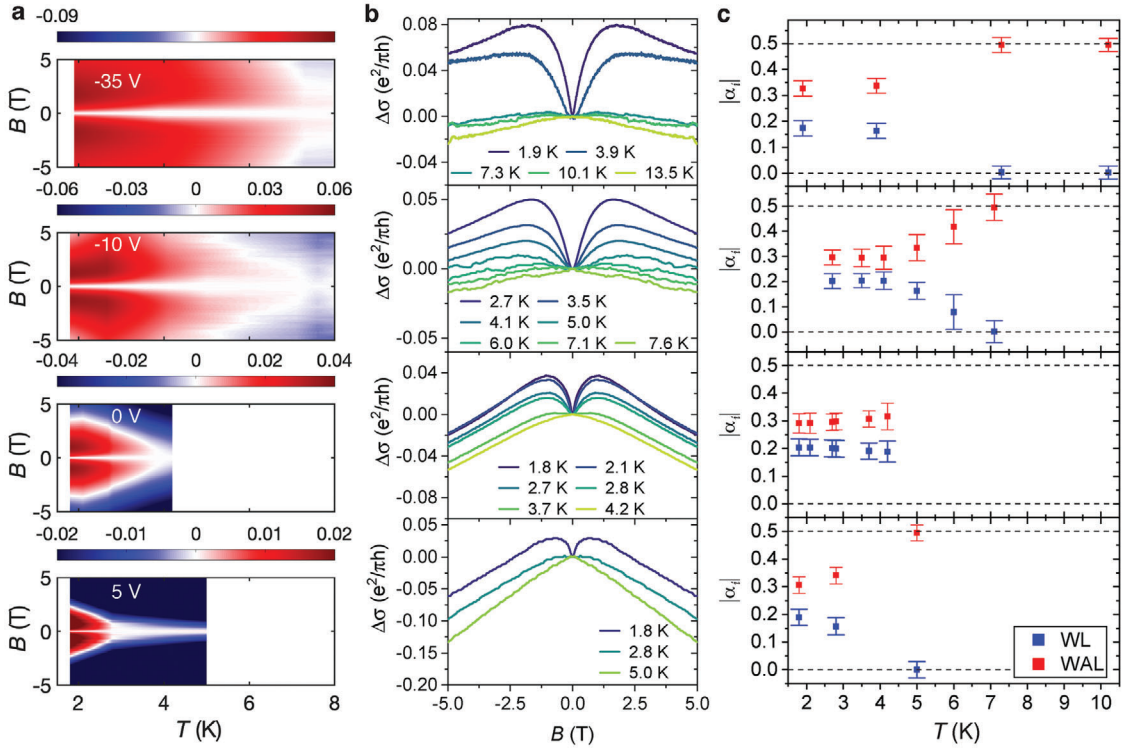

Figure 3. MC data as function of the temperature at Vg = –35, –10, 0, and 5 V shown as a) color map and b) bare MC versus B data. c) Fit parameters α_i (i = 0,1) using Equation (1). The fits show that α_1 goes to zero above 7–8 K, i.e., at a temperature similar to the FM Tc. The error-bars are evaluated by fitting the data in different field-ranges and by estimating the corresponding confidence intervals of each parameter (see Figure S8, Supporting Information and Statistical Methods).

non-trivial Berry curvature (Figure 4b) and a hot-spot at the avoided crossing between the two Rashba-SOC spin-split bands ref. [16].

In order to confirm the overall picture provided by the minimal model, we performed calculations also using the full Hamiltonian tight binding approach, which better reproduces the snowflake shape of the Fermi surfaces. As shown in Figure 4(c,d), the full Hamiltonian tight binding calculations confirm the emergence of a non-trivial Berry curvature and give an even stronger evidence of a hot-spot at the avoided crossing between the two Rashba-SOC spin-split bands (related spin textures shown in Figure S7b–d, Supporting Information). It is worth noting that the additional Zeeman splitting in the perpendicular magnetic field might enforce the magnetic gap due to progressive alignment of the magnetic moments. However, the Zeeman field alone appears insufficient to explain the MC anomaly, as it was never observed in the (001) LAO/ETO/STO 2DES. Thus, we conclude that hexagonal warping in (111) heterostructures is crucial to describe our results.

The evolution with the gate-voltage of the anomalous MC-data in the (111) LAO/ETO/STO 2DES can be, then, directly related to the tuning of the chemical potential: a maximum of the

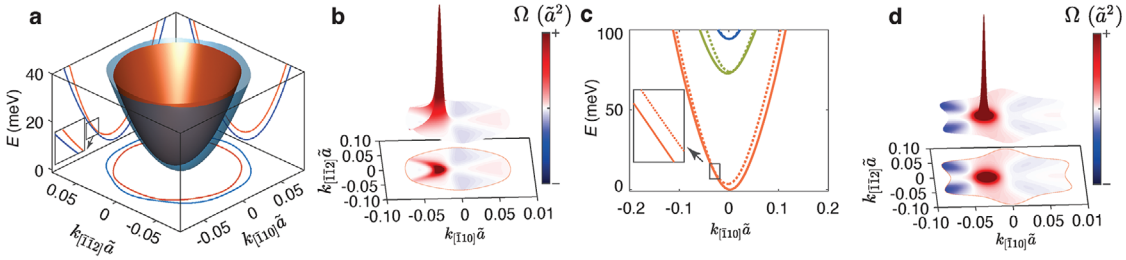

Figure 4. a) Energy bands in the presence of a planar exchange field with the direction along $[\bar{1}\bar{1}2]$. Lowest Rashba-spin split energy bands and b) Berry curvature at E_F = 60 meV of a spin-split band analytically evaluated from the minimal model described in the main text. The calculations show the emergence of a hot-spot, i.e., a non-trivial Berry phase, near the Dirac-like point. Tight-binding Hamiltonian calculations, beyond the minimal model, of c) the electronic bands along $[\bar{1}10]$ and of d) the non-trivial Berry curvature. The avoided crossing of the bands and the opening of a magnetic gap are magnified in the insets of panels (a,c).

peak-shoulder feature associated to the competing WL and WAL terms is attained when the chemical potential approaches the hot-spot, while departing from it drives the gradual reduction. Thus, the MC is strongly affected by the back-scattering of the Dirac-like fermions, experiencing a non-trivial Berry phase along self-crossing loops. This behavior, already established in gapped 3D-TIs,[4–6] was rarely found in other 2DESs, since it requires the simultaneous presence of a large Rashba-like SOC, a sizable gap Δ due to TRS-breaking, and very low chemical potential.[4]

3. Conclusion

Our work establishes a method to create oxide 2DES characterized by transport properties mimicking those of systems hosting Dirac fermions, as in gapped 3D-TIs. The simultaneous presence of Rashba-SOC, magnetic correlations, and the hexagonal symmetry of the system with enhanced trigonal crystal field splitting, allows the tuning of the 2DES chemical potential near a Dirac-like point generated by the spin-split lowest energy bands. This triggers a Berry-curvature hot-spot and topological charges in the 2DES without the need of external planar magnetic field, which on the other hand is needed in the case of non-magnetic 2DES, e.g., in (111) LAO/STO and $LaTiO_3$/STO.[16,17] Similar approaches can be envisaged in the case of other novel interfaces, including 2D-atomic non-magnetic/magnetic bi-layers and other oxide 2DES, alike $KTaO_3$ (111) based-2DES,[31,32] opening a vast space for exploration at the intersection between topology and correlations of interest for spin-orbitronics[33,34] and topological electronics.

4. Experimental Section

Sample Growth: Epitaxial LAO/ETO heterostructures were deposited on Ti-terminated STO(111) single crystals using pulsed laser deposition (PLD) assisted by reflection high energy electron diffraction (RHEED)[19] at 720 °C and in a background oxygen pressure of 7.5×10^{-5} mbar. A KrF excimer laser with 248 nm wavelength and 1 Hz repetition was focused on sintered $Eu_2Ti_2O_7$ target and on a crystalline LAO target at a fluence of 1.3 Jcm^{-2}. The sequential deposition of ETO (3 uc) and LAO (14 uc) films on Ti-terminated (111) STO single crystal was monitored by the oscillations of the specular RHEED intensity (Figure S1a, Supporting Information). The 300 $\mu m \times$ 100 μm Hall bars were realized by a combination of optical lithography and cold ion milling, following the procedure described in ref. [18].

Magneto-Transport Measurements: Magneto-transport measurements were performed in a He^4 flow cryostat using standard lock-in amplifiers (f = 10 Hz and j_{RMS} = 100 nA). The longitudinal and transverse voltages were measured simultaneously. The magnetic field was swept in the ± 12 T range. Data as function of the back-gate were acquired in a +30 V to −120 V range. The leakage current across the (111) STO gate-oxide was below 1 nA. The sheet resistance saturates above +30 V. MC and Hall effect data were also acquired at different temperatures in the 1.8–15 K range.

XMCD and SQUID Magnetization Measurements: Eu-$M_{4,5}$ edge XAS spectra were acquired at the Extreme beamline of the PSI-SLS and at the ID32 ESRF synchrotron facilities using the total electron yield (TEY) method (see ref. [19]). The magnetic-field-dependent magnetization loops were obtained by measuring, at each field, the difference between the TEY intensities at the M_5-Eu edge peaks obtained with two different helicities (combination of polarization and field direction), and normalized to the background acquired at an energy below the absorption edge. SQUID data were collected by using a Quantum Design MPMS3 magnetometer at the Université de Strasbourg, IPCMS. The data were corrected for the STO diamagnetism subtracting the high field linear contribution.

Statistical Methods: The standard symmetrization procedure was used to remove any (minor) contribution of the transverse resistance to the longitudinal magnetoresistance. The MC data in Figures 2 and 3 have been fitted using Equation (1) by least squares fit. The error-bars for the fitting parameters correspond to the confidence intervals for the mean predictions of each parameter.

Supporting Information

Supporting Information is available from the Wiley Online Library or from the author.

Acknowledgements

The authors thank Cedric Bray for technical assistance, the staff of the ID32 beamline of the European Synchrotron Radiation Facility and that of the X-Treme of the Swiss Light Source. This project received funding from the European Union's Horizon Europe research and innovation programme project IQARO, under grant agreement n. 101115190, by the Ministry of University and Research project PRIN 2022 SONATA, No. P2022SB73K, funded by the EU—Next Generation EU, and PRIN 2022 STIMO, No. 2022TWZ9NR. M.S. and Y.C. acknowledge financial support from PNRR MUR project PE0000023-NQSTI. M.T. acknowledges financial support from "Fondazione Angelo Della Riccia". D.P. thanks the French National Research Agency (ANR) through the ANR-JCJC FOXIES ANR-21-CE08-0021.

Open access publishing facilitated by Consiglio Nazionale delle Ricerche, as part of the Wiley - CRUI-CARE agreement.

Conflict of Interest

The authors declare no conflict of interest.

Data Availability Statement

The data that support the findings of this study are available from the corresponding author upon reasonable request.

Keywords

Berry phase/curvature, ferromagnetic 2DES, weak anti-localization, weak localization

Received: July 17, 2024
Revised: October 14, 2024
Published online: October 30, 2024

[1] F. D. M. Haldane, *Phys. Rev. Lett.* **1988**, *61*, 2015.
[2] R. Yu, W. Zhang, H.-J. Zhang, S.-C. Zhang, X. Dai, Z. Fang, *Science* **2010**, *329*, 61.
[3] B. A. Bernevig, T. L. Hughes, S.-C. Zhang, *Science* **2006**, *314*, 1757.
[4] H. Z. Lu, J. Shi, S. Q. Shen, *Phys. Rev. Lett.* **2011**, *107*, 076801.
[5] M. Liu, J. Zhang, C.-Z. Chang, Z. Zhang, X. Feng, K. Li, K. He, L.-l. Wang, X. Chen, X. Dai, Z. Fang, Q.-K. Xue, X. Ma, Y. Wang, *Phys. Rev. Lett.* **2012**, *108*, 036805.
[6] M. Lang, L. He, X. Kou, P. Upadhyaya, Y. Fan, H. Chu, Y. Jiang, J. H. Bardarson, W. Jiang, E. S. Choi, Y. Wang, N. C. Yeh, J. Moore, K. L. Wang, *Nano Lett.* **2013**, *13*, 48.

[7] L. Fu, *Phys. Rev. Lett.* **2009**, *103*, 266801.
[8] M. V. Berry, *Proc. R. Soc. Lond A* **1984**, *392*, 45.
[9] S. Q. Shen, *Phys. Rev. B* **2004**, *70*, 081311.
[10] A. D. Caviglia, S. Gariglio, N. Reyren, D. Jaccard, T. Schneider, M. Gabay, S. Thiel, G. Hammerl, J. Mannhart, J. M. Triscone, *Nature* **2008**, *456*, 624.
[11] D. Stornaiuolo, C. Cantoni, G. M. De Luca, R. Di Capua, E. Di Gennaro, G. Ghiringhelli, B. Jouault, D. Marrè, D. Massarotti, F. M. Granozio, I. Pallecchi, C. Piamonteze, S. Rusponi, F. Tafuri, M. Salluzzo, *Nature Materials* **2016**, *15*, 278.
[12] P. K. Rout, E. Maniv, Y. Dagan, *Phys. Rev. Lett.* **2017**, *119*, 237002.
[13] J. Bréhin, Y. Chen, M. D. Antuono, S. Varotto, D. Stornaiuolo, C. Piamonteze, J. Varignon, M. Salluzzo, M. Bibes, *Nat. Phys.* **2023**, *19*, 823.
[14] R. Di Capua, M. Verma, M. Radovic, V. N. Strocov, C. Piamonteze, E. B. Guedes, N. C. Plumb, Y. Chen, M. D'Antuono, G. M. De Luca, E. Di Gennaro, D. Stornaiuolo, D. Preziosi, B. Jouault, F. Miletto Granozio, A. Sambri, R. Pentcheva, G. Ghiringhelli, M. Salluzzo, *npj Quantum Mater.* **2022**, *7*, 41.
[15] P. He, S. M. K. Walker, S. S. Zhang, F. Y. Bruno, M. S. Bahramy, J. M. Lee, R. Ramaswamy, K. Cai, O. Heinonen, G. Vignale, F. Baumberger, H. Yang, *Phys. Rev. Lett.* **2018**, *120*, 266802.
[16] E. Lesne, Y. G. Sağlam, R. Battilomo, M. T. Mercaldo, T. C. van Thiel, U. Filippozzi, C. Noce, M. Cuoco, G. A. Steele, C. Ortix, A. D. Caviglia, *Nat. Mater.* **2023**, *22*, 576.
[17] G. Tuvia, A. Burshtein, I. Silber, A. Aharony, O. Entin-Wohlman, M. Goldstein, Y. Dagan, *Phys. Rev. Lett.* **2024**, *132*, 146301.
[18] M. D'Antuono, A. Kalaboukhov, R. Caruso, S. Wissberg, S. Weitz Sobelman, B. Kalisky, G. Ausanio, M. Salluzzo, D. Stornaiuolo, *Nanotechnology* **2022**, *33*, 085301.
[19] Y. Chen, M. D'Antuono, N. B. Brookes, G. M. D. Luca, R. D. Capua, E. D. Gennaro, G. Ghiringhelli, C. Piamonteze, D. Preziosi, B. Jouault, M. Cabero, J. M. González-Calbet, C. León, J. Santamaria, A. Sambri, D. Stornaiuolo, M. Salluzzo, *ACS Appl. Electron. Mater.* **2022**, *4*, 3226.
[20] D. Xiao, W. Zhu, Y. Ran, N. Nagaosa, S. Okamoto, *Nat. Commun.* **2011**, *2*, 596.
[21] D. Doennig, W. E. Pickett, R. Pentcheva, *Phys. Rev. Lett.* **2013**, *111*, 126804.
[22] U. Khanna, P. K. Rout, M. Mograbi, G. Tuvia, I. Leermakers, U. Zeitler, Y. Dagan, M. Goldstein, *Phys. Rev. Lett.* **2019**, *123*, 36805.
[23] M. Trama, V. Cataudella, C. A. Perroni, F. Romeo, R. Citro, *Phys. Rev. B* **2022**, *106*, 075430.
[24] G. M. De Luca, R. Di Capua, E. Di Gennaro, A. Sambri, F. M. Granozio, G. Ghiringhelli, D. Betto, C. Piamonteze, N. B. Brookes, M. Salluzzo, *Phys. Rev. B* **2018**, *98*, 115143.
[25] V. K. Dugaev, P. Bruno, J. Barnaś, *Phys. Rev. B* **2001**, *64*, 144423.
[26] A. D. Caviglia, M. Gabay, S. Gariglio, N. Reyren, C. Cancellieri, J. M. Triscone, *Phys. Rev. Lett.* **2010**, *104*, 126803.
[27] S. Hikami, A. I. Larkin, Y. Nagaoka, *Progress of Theoretical Physics* **1980**, *63*, 707.
[28] S. V. Iordanskii, Y. B. Lyanda-Geller, G. E. Pikus, *JETP Lett.* **1994**, *60*, 206.
[29] S. Maekawa, H. Fukuyama, *J. Phys. Soc. Jpn.* **1981**, *50*, 2516.
[30] D. Stornaiuolo, B. Jouault, E. Di Gennaro, A. Sambri, M. D'Antuono, D. Massarotti, F. M. Granozio, R. Di Capua, G. M. De Luca, G. P. Pepe, F. Tafuri, M. Salluzzo, *Phys. Rev. B* **2018**, *98*, 075409.
[31] C. Liu, X. Yan, D. Jin, Y. Ma, H.-W. Hsiao, Y. Lin, T. M. Bretz-Sullivan, X. Zhou, J. Pearson, B. Fisher, J. S. Jiang, W. Han, J.-M. Zuo, J. Wen, D. D. Fong, J. Sun, H. Zhou, A. Bhattacharya, *Science* **2021**, *371*, 716.
[32] H. Xu, H. Li, N. Gauquelin, X. Chen, W. F. Wu, Y. Zhao, L. Si, D. Tian, L. Li, Y. Gan, S. Qi, M. Li, F. Hu, J. Sun, D. Jannis, P. Yu, G. Chen, Z. Zhong, M. Radovic, J. Verbeeck, Y. Chen, B. Shen, *Adv. Mater.* **2024**, 2313297.
[33] E. Lesne, Y. Fu, S. Oyarzun, J. C. Rojas-Sánchez, D. C. Vaz, H. Naganuma, G. Sicoli, J. P. Attané, M. Jamet, E. Jacquet, J. M. George, A. Barthélémy, H. Jaffrès, A. Fert, M. Bibes, L. Vila, *Nat. Mater.* **2016**, *15*, 1261.
[34] L. M. Vicente-Arche, J. Bréhin, S. Varotto, M. Cosset-Cheneau, S. Mallik, R. Salazar, P. Noël, D. C. Vaz, F. Trier, S. Bhattacharya, A. Sander, P. Le Fèvre, F. Bertran, G. Saiz, G. Ménard, N. Bergeal, A. Barthélémy, H. Li, C. C. Lin, D. E. Nikonov, I. A. Young, J. E. Rault, L. Vila, J. P. Attané, M. Bibes, *Adv. Mater.* **2021**, *33*, 2102102.